SURFACE CHEMISTRY

Real-time imaging of adatom-promoted graphene growth on nickel

Laerte L. Patera,[1,2]* Federico Bianchini,[1,3] Cristina Africh,[2]† Carlo Dri,[1,2]‡ German Soldano,[4] Marcelo M. Mariscal,[4] Maria Peressi,[1,5]† Giovanni Comelli[1,2]

Single adatoms are expected to participate in many processes occurring at solid surfaces, such as the growth of graphene on metals. We demonstrate, both experimentally and theoretically, the catalytic role played by single metal adatoms during the technologically relevant process of graphene growth on nickel (Ni). The catalytic action of individual Ni atoms at the edges of a growing graphene flake was directly captured by scanning tunneling microscopy imaging at the millisecond time scale, while force field molecular dynamics and density functional theory calculations rationalize the experimental observations. Our results unveil the mechanism governing the activity of a single-atom catalyst at work.

Reduced dimensionality in the catalyst structure often leads to increased chemical reactivity (*1*, *2*). More specifically, atomic steps of metal surfaces were experimentally identified as the active sites for several heterogeneous catalytic reactions (*3*, *4*), and this identification was theoretically rationalized in terms of a characteristic upshift of the d-band center (*5*). Such undercoordinated sites play also a crucial role in governing the stability of the active phase (*4*). Single atoms, representing the lowest possible coordination, can exhibit even higher specificity and efficiency compared to stepped surfaces (*1*). For example, isolated single metal atoms anchored onto oxide nanocrystallites promote CO oxidation (*6*) and the water–gas-shift reaction (*7*). Recent studies also revealed the peculiar activity of single-atom alloys in boosting the selective hydrogenation of alkenes and hydrocarbons (*8*).

Mobile adatoms, commonly present on metal surfaces at elevated temperatures, are involved in several chemical processes occurring on surfaces and at the solid-liquid interface (*9*, *10*). However, the lack of direct experimental observation of the dynamics of these peculiar processes at the atomic scale, generally owing to the difficulty of achieving simultaneous spatial and temporal resolution, limits the description and understanding of the surface reaction pathways. For the specific case of the chemical vapor deposition (CVD) growth of graphene on transition metals, a catalytic role of single metal atoms was predicted by theorists, but the detailed growth mechanism at the atomic scale remains unclear (*11*).

Nickel (Ni) is one of the most used substrates to synthesize graphitic carbon single layers (*12*). We report the characterization of graphene growth on Ni(111) in real time by means of in situ high-speed scanning tunneling microscopy (STM) measurements. By monitoring the layer formation at the atomic scale and with a time resolution down to milliseconds, we observed at the kink sites of the graphene edges single Ni atoms that are directly involved in the growth process. Simulations of possible reaction paths based

[1]Department of Physics, University of Trieste, Via Valerio 2, I-34127 Trieste, Italy. [2]Istituto Officina dei Materiali–Consiglio Nazionale delle Ricerche (IOM-CNR) Laboratorio TASC, S.S. 14 km 163.5 in AREA Science Park, Basovizza, I-34149 Trieste, Italy. [3]Centre for Materials Science and Nanotechnology (SMN), Department of Chemistry, University of Oslo, Post Office Box 1126, N-0318 Oslo, Norway. [4]Instituto de Investigaciones en Físico-Química de Córdoba, Consejo Nacional de Investigaciones Científicas y Técnicas (INFIQC CONICET) and Departamento de Química Teorica y Computacional, Facultad de Ciencias Quimicas, Universidad Nacional de Córdoba, Cdad. Universitaria, 5000 Córdoba, Argentina. [5]Istituto Officina dei Materiali–Consiglio Nazionale delle Ricerche (IOM-CNR) DEMOCRITOS National Simulation Center, via Bonomea 265, I-34136 Trieste, Italy. *Present address: Institute of Experimental and Applied Physics, University of Regensburg, D-93053 Regensburg, Germany. **†Corresponding author. Email: africh@iom.cnr.it (C.A.); peressi@ts.infn.it (M.P.)** ‡Present address: ELETTRA-Sincrotrone Trieste, S.S. 14 km 163.5, Basovizza, I-34149 Trieste, Italy.

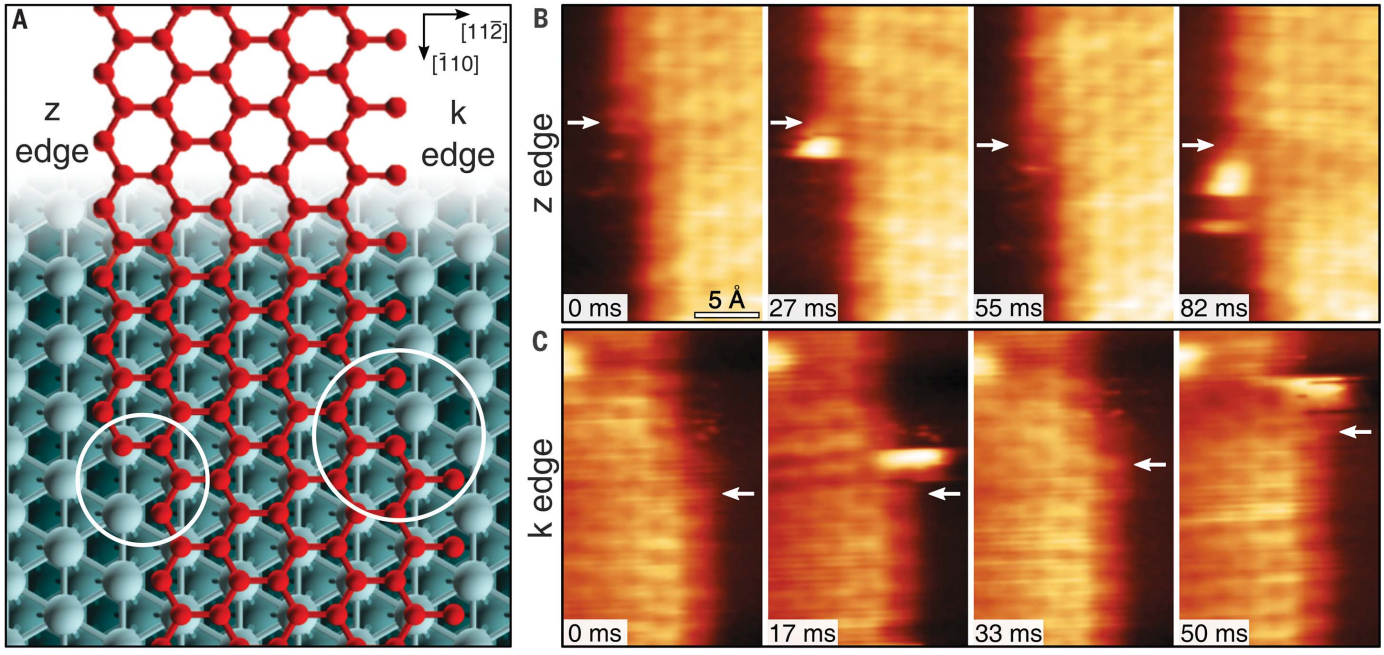

Fig. 1. Graphene growth along z and k edges. (**A**) Zigzag (z) and Klein (k) edges of a top-fcc EG layer on Ni (111). At both edges, the kink structures are highlighted by circles. (**B**) High-speed STM sequence acquired at 710 K in quasi-constant height mode at the z edge, from movie S1 (V = 20 mV; I = 8 nA; frame rate = 36.5 Hz]. White arrows indicate the position of C atoms in fcc-hollow sites near the kink. (**C**) Same as in (B) but for the k edge, from movie S2 (V = 20 mV; I = 7 nA; frame rate = 60 Hz).

on density functional theory (DFT) revealed that Ni adatoms drive the carbon (C) atom addition mechanism by substantially lowering the corresponding reaction barriers.

Islands of monolayer epitaxial graphene (EG) were synthesized on Ni(111) by subsurface C segregation at temperatures between 700 and 740 K (*13*). Three coexisting stable chemisorbed configurations of EG were observed (*14*), with the top/face-centered cubic geometry (top-fcc) as the most abundant phase. During growth, the island edges evolved too rapidly to be resolved by standard STM imaging (typical image acquisition rates of ≈0.02 frames/s). Nevertheless, in a previous study, we succeeded in identifying the top-fcc edge structure by performing high-speed STM measurements (*15*), exploiting the FAST module developed in our laboratory (*16*, *17*). The module allows for image acquisition rates up to 100 frames/s with commercial microscopes already optimized for structural and reactivity studies. The edge terminations of EG islands on Ni(111) during growth at temperatures higher than 570 K (*15*) were identified as the zigzag (z) and Klein (k) structures shown in Fig. 1A. For both edges, kink sites obtained by interrupting the last two C rows were predicted to play an important role in graphene edge expansion (*18*, *19*).

To identify the underlying growth mechanisms during the C-attachment process at both edges, we acquired STM movies with high spatial and temporal resolution and long enough for a statistically relevant analysis.

Series of consecutive images along z [movie S1 (*20*)] and k (movie S2) edges were acquired with frame rates of 36.5 and 60 Hz, respectively. The use of different frame rates (from 4 to 10 Hz) and tunneling current setpoints (from 500 pA to 10 nA) did not yield substantial differences, indicating a negligible effect of the fast scanning tip on the observed processes. This consistency presumably resulted from the short tip-surface interaction time (typically ≈1.5 to 10 μs/ pixel) and from the thermal excitation that at elevated temperatures likely overwhelmed tip-induced effects (*21*).

Movie S1 initially shows the formation at the z edge of two kink sites, acting as nucleation centers for graphene growth (fig. S1). In the image sequence in Fig. 1B, growth proceeds from the kink site in the middle by orderly completion of the two interrupted carbon rows while moving the kink ahead. During the z edge growth, the observed structure of the kink remains equivalent to the initial one, probably because of the preference for fcc-hollow site termination (*15*). A similar evolution was predicted by previous DFT calculations for the z edge of EG on Cu(111), where the growth would start from the hexagon forming the kink, and continuous incorporation of C atoms would form a new z chain on the graphene growth front (*19*). The image sequence in Fig. 1C, extracted from movie S2, shows the growth mechanism at the k edge, similar to the one described above for the z edge, i.e., proceeding from the kink site and parallel to the edge. Our DFT calculations (fig. S2) support this observation, showing that the incorporation of new C atoms takes place at the kink and that, after addition of a first C atom in a top site, the energetics favor the addition of a second C atom in a fcc-hollow site.

A closer examination of both sequences in Fig. 1, B and C, reveals the presence of bright objects at the kink sites. These features appeared and disappeared: They were present in some frames (at 27 and 82 ms in Fig. 1B, and at 17 and 50 ms in Fig. 1C) and were absent in others (at 0 and 55 ms in Fig. 1B, and at 0 and 33 ms in Fig. 1C). They were typically imaged for few scanlines only, indicating a short residence time of the originating species (at the millisecond time scale; see supplementary text), and their appearance did not depend on scanning parameters and tip conditions. Regarding the nature of the imaged species, one possibility would be that they are mobile C clusters, as described for graphene growth on Ru(0001) and Rh(111) (*22*, *23*). However, for Rh(111), where STM images have been acquired, the clusters have a height similar to that of the graphene layer, at variance with what

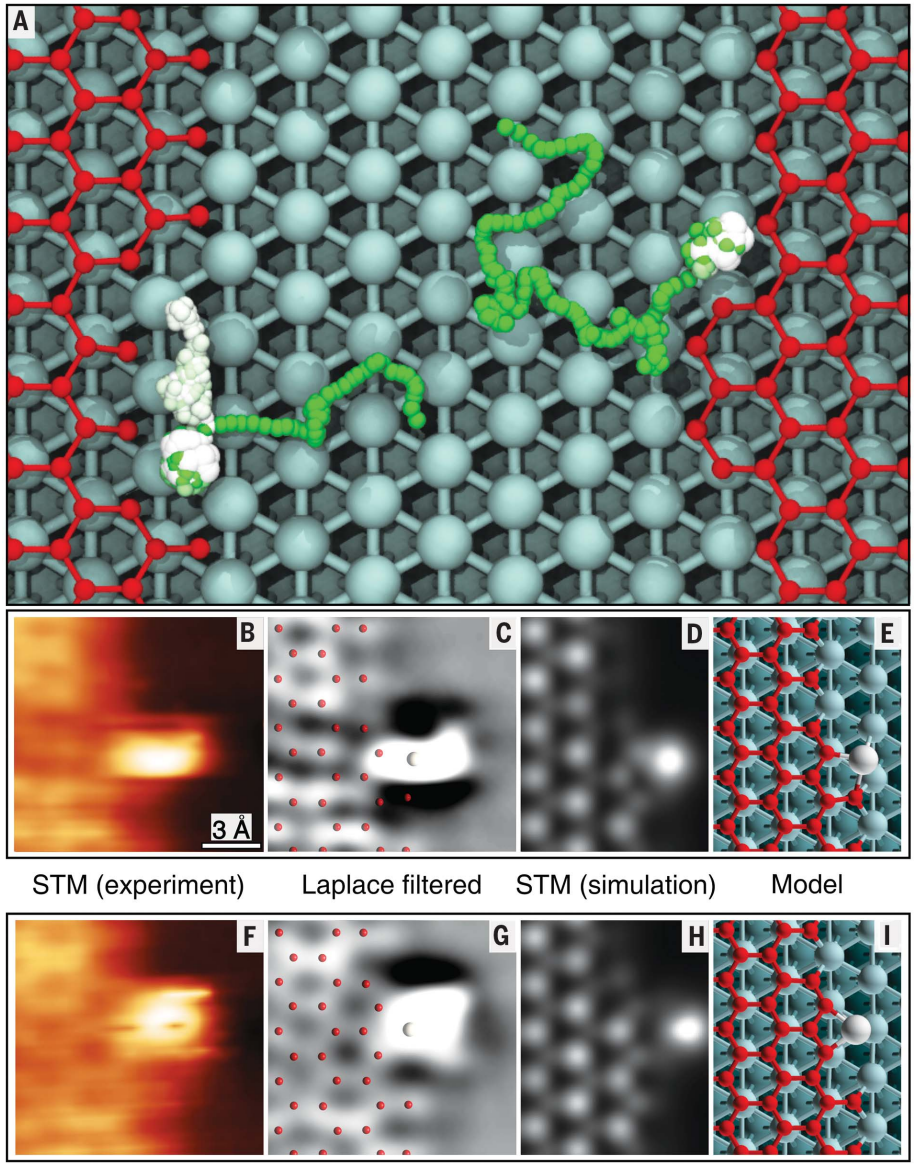

Fig. 2. Nickel adatoms at the graphene edges. (**A**) Ni adatom diffusing on a surface in a region delimited by graphene z (right) and k (left) edges with kinks. Two representative trajectories obtained by MD simulations with ReaxFF performed at 710 K for 100 ps are shown. Color palette for Ni trajectories: from green (initial position) to white (final position). The final steps are highlighted by increasing the ball size. (**B** to **I**) Short-lived configurations of Ni adatom at k-edge kinks: (B and F) High-speed STM images from movie S2 (*20*) (V = 20 mV; I = 7 nA); (C and G) Laplace-filtered version of images from (B) and (F) with superimposed ball models; (D and H) constant-height STM simulated images based on the calculated geometries (E and I).

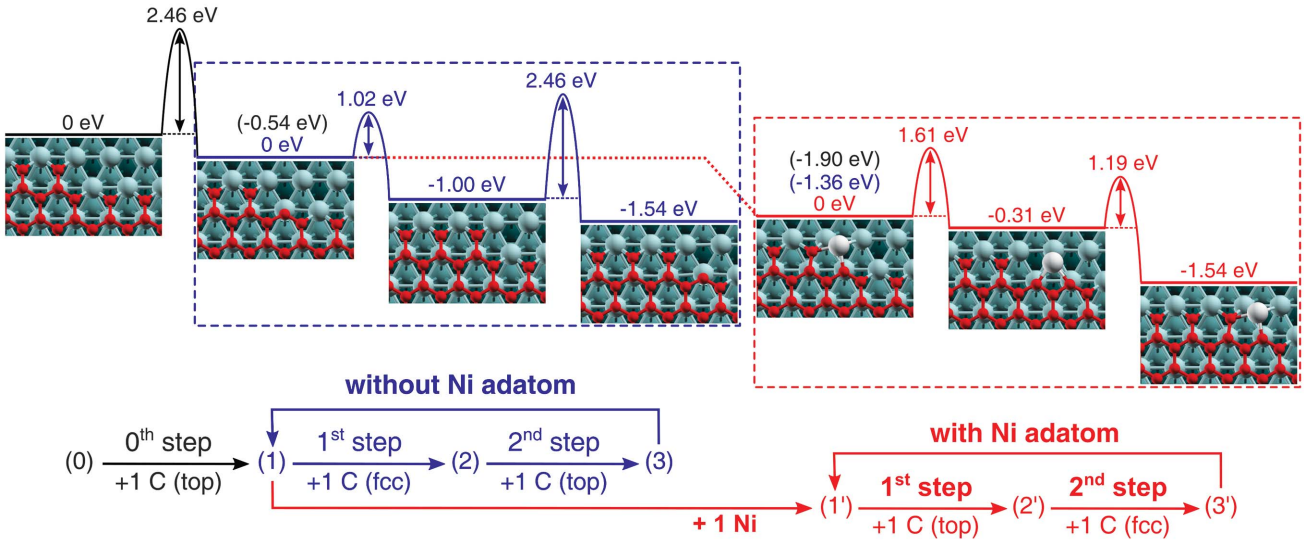

Fig. 3. Alternative graphene growth pathways as predicted by DFT. Energy zero corresponds to the bare kink configuration (0), plus one Ni adatom on the surface far from the edge and a reservoir of sub-fcc C atoms far from the edge. For clarity, the energy scale is reset for each cycle, producing the blue and red energy scales, respectively.

we observe. Apparent height and lateral dimensions of the mobile species are, on the contrary, comparable to those of the static pointlike defects observed after CVD graphene growth on Ni(111) in the same temperature range, which were previously identified as substitutional Ni atoms trapped in the graphene network during the growth process (*13*). We therefore attribute the bright features in Fig. 1, B and C, to mobile Ni adatoms, in line with previous DFT-based prediction (*24*). This hypothesis is supported by the well-known presence of diffusing adatoms on metal surfaces at elevated temperatures (*25*). Other dashed features with lower apparent height (comparable to or lower than that of carbon atoms in graphene) were visible in some frames and can be attributed either to Ni imaged by the tip in an off-center position (*26*), or to moving C atoms. A further confirmation of our identification of the bright features in the STM images as Ni adatoms comes from molecular dynamics (MD) simulations with state-of-the-art reactive force field (ReaxFF) performed at 710 K [Fig. 2A; details in (*20*)]. Mobile Ni adatoms moved randomly over the bare metal surface until they reached a graphene edge. There, they diffused parallel to the edge, with considerably longer residence time in the kink sites.

A notable feature in the STM image series is that the presence of the Ni adatoms at the kinks is in most of the cases accompanied by C dimer attachment nearby (see frame at 55 ms in Fig. 1B, and frames at 33 and 50 ms in Fig. 1C), suggesting a catalytic role of the single metal atom. This observation is consistent with previous DFT calculations for graphene on Cu(111) (*19*), which showed that the barrier for C incorporation at the z edge was strongly reduced by Cu adatom passivation at armchair-like sites, present near a hexagon (a kink) sticking out of the edge. Our interpretation is also in line with recent in situ transmission electron microscopy reports of the chemical activity of single atoms in facilitating addition and removal of C atoms from the edges of suspended graphene flakes (*27*). These previous results, although notable, are not related to a real growth process, but rather are related to attachment-detachment events of individual C atoms, and thus cannot be directly extended to technologically relevant CVD growth processes on solid metal surfaces.

That the Ni adatoms were almost exclusively imaged at the kink sites suggests that they represent a minimum-energy configuration for Ni; nevertheless, the short residence time implies that the bond can be easily broken at these temperatures, avoiding the poisoning of the active kink site. No stable Ni trapping was observed in our time series, at variance with the defect formation pathway predicted by Wang *et al.* (*24*).

From the STM sequence corresponding to the k edge, two short-lived Ni adatom configurations can be identified at the kink sites (Fig. 2, B, C, F, and G). DFT simulations of these configurations yielded the two stable structures shown in Fig. 2, E and I, where a Ni adatom and one or two top C atoms were added to the bare kink. The corresponding constant-height simulated images in Fig. 2, D and H, match the experimental STM data. DFT calculations indicate a pronounced mutual stabilization effect between C and Ni adatoms at the kink (from the energy comparison of configurations in figs. S2 and S3). These results suggest that Ni had a strong promoting role in the addition of C atoms to the kink and hence in the edge growth, as previously predicted for Cu(111) (*19*). Similar conclusions could be drawn for the z edge, where a single intermediate state was imaged and described by DFT calculations (fig. S4).

The stable configurations observed by STM and confirmed by theory can serve as a guide for a DFT description of the entire growth process, discriminating among many possible alternative paths and highlighting the catalytic role of the Ni adatom. In Fig. 3, we report the energy diagram corresponding to selected C-attachment pathways to the k edge with and without the presence of the Ni adatom. The energy gain upon addition of a C atom is referred to a subsurface position far from the edge ["sub-fcc," which is the most stable position on a clean Ni(111) surface]; for the addition of a Ni adatom, to a position on the surface far from the edge.

We take as initial configuration [labeled (0) in Fig. 3] a k edge with all terminating C atoms in fcc-hollow. The addition of a first C atom on the top site (1) involves a considerable energy barrier, 2.46 eV. The growth process can then follow two alternative cycles, either without (blue box) or with (red box) a Ni adatom.

Considering the process without a Ni adatom, the attachment of the second C atom in a fcc-hollow position (2) requires overcoming a barrier of 1.02 eV (see fig. S5 for details on energy barriers). Because of the epitaxial match between graphene and Ni(111), the edge configuration is now equivalent to the initial one. Further addition of a C top atom (3) requires again overcoming the 2.46-eV barrier, completing the cycle that can be repeated in a continuous loop, but always including this high energy barrier.

In the alternative path, a Ni adatom attaches without an energy barrier to the kink decorated by the top C atom (1), yielding an energy gain of 1.36 eV (1′). The most favorable configuration for attachment of a second C atom is again a top site, with the Ni adatom diffusing laterally, bonding to the two top C atoms (2′). In the last step of the growth cycle, another C atom attaches

in the fcc-hollow position, extending the graphene edge and pushing aside the Ni adatom (3′). The energy barriers involved in the two steps of this cycle are 1.61 and 1.19 eV, respectively. Ni adatoms, spontaneously binding to the kink site, thus reduce the rate-limiting energy barrier of the cyclic process by about 35% (from 2.46 to 1.61 eV), acting as single-atom catalysts for the graphene growth process.

Because the Ni attachment is barrierless, the detachment barriers from the two stable states at the kink are 1.36 and 1.35 eV, obtained as the DFT energy differences of the corresponding equilibrium states, i.e., configurations (1′) and (2′) of Fig. 3, and configurations (1) in Fig. 3 and (e) in fig. S2, respectively. These values yield Ni residence time values on the millisecond scale, compatible with the values extracted from the STM data (fig. S6).

REFERENCES AND NOTES

1. X. F. Yang *et al*., *Acc. Chem. Res.* **46**, 1740–1748 (2013).
2. A. Baraldi *et al*., *J. Phys. Chem. C* **115**, 3378–3384 (2011).
3. T. Zambelli, J. Wintterlin, J. Trost, G. Ertl, *Science* **273**, 1688–1690 (1996).
4. B. L. M. Hendriksen *et al*., *Nat. Chem.* **2**, 730–734 (2010).
5. B. Hammer, J. K. Nørskov, *Nature* **376**, 238–240 (1995).
6. B. Qiao *et al*., *Nat. Chem.* **3**, 634–641 (2011).
7. J. Lin *et al*., *J. Am. Chem. Soc.* **135**, 15314–15317 (2013).
8. G. Kyriakou *et al*., *Science* **335**, 1209–1212 (2012).
9. Y. C. Yang, A. Taranovskyy, O. M. Magnussen, *Angew. Chem. Int. Ed.* **51**, 1966–1969 (2012).
10. Z. Feng *et al*., *ACS Nano* **9**, 8697–8709 (2015).
11. X. Zhang, J. Xin, F. Ding, *Nanoscale* **5**, 2556–2569 (2013).
12. R. Rosei *et al*., *Phys. Rev. B* **28**, 1161–1164 (1983).
13. L. L. Patera *et al*., *ACS Nano* **7**, 7901–7912 (2013).
14. F. Bianchini, L. L. Patera, M. Peressi, C. Africh, G. Comelli, *J. Phys. Chem. Lett.* **5**, 467–473 (2014).
15. L. L. Patera *et al*., *Nano Lett.* **15**, 56–62 (2015).
16. F. Esch *et al*., *Rev. Sci. Instrum.* **82**, 053702 (2011).
17. https://fastmodule.iom.cnr.it/
18. V. I. Artyukhov, Y. Liu, B. I. Yakobson, *Proc. Natl. Acad. Sci. U.S.A.* **109**, 15136–15140 (2012).
19. H. Shu, X. Chen, X. Tao, F. Ding, *ACS Nano* **6**, 3243–3250 (2012).
20. See supplementary materials.
21. T. Mitsui, M. K. Rose, E. Fomin, D. F. Ogletree, M. Salmeron, *Science* **297**, 1850–1852 (2002).
22. E. Loginova, N. Bartelt, P. J. Feibelman, K. F. McCarty, *New J. Phys.* **10**, 093026 (2008).
23. B. Wang *et al*., *J. Phys. Chem. C* **121**, 9413–9423 (2017).
24. L. Wang, X. Zhang, H. L. W. Chan, F. Yan, F. Ding, *J. Am. Chem. Soc.* **135**, 4476–4482 (2013).
25. G. Ehrlich, *Surf. Sci.* **246**, 1–12 (1991).
26. J. Wintterlin *et al*., *Surf. Sci.* **394**, 159–169 (1997).
27. J. Zhao *et al*., *Proc. Natl. Acad. Sci. U.S.A.* **111**, 15641–15646 (2014).

ACKNOWLEDGMENTS

We thank C. Cepek, J. Repp, and A. Peronio for fruitful discussions and K. C. Prince for carefully reading our manuscript. We thank the Detectors and Instrumentation Group at ELETTRA-Sincrotrone Trieste and F. Esch for their contribution to the FAST module development. **Funding:** We acknowledge funding from the EU-H2020 Research and Innovation programme under grant agreement no. 654360 Nanoscience Foundries and Fine Analysis-Europe; Italian Ministry of Foreign Affairs, through the Executive Programme with Argentina 2014–2016 (PGR00190); University of Trieste through the program "Finanziamento di Ateneo per progetti di ricerca scientifica–FRA 2015"; Consejo Nacional de Investigaciones Científicas y Técnicas (CONICET), Fondo para la Investigación Científica y Tecnológica (FONCyT) PICT-2015-2191, and Secretaría de Ciencia y Tecnología (SeCyT)-Universidad Nacional de Córdoba (UNC) (Argentina). Computational resources were obtained from the CINECA Italian Consortium of Universities through the Italian SuperComputing Resource Allocation (ISCRA) initiative and the agreement with the University of Trieste and from Centro de Computación de Alto Desempeño (CCAD), Universidad Nacional de Córdoba (Argentina). **Author contributions:** L.L.P. and C.A. conceived the experiments. L.L.P performed the experiments and analyzed the experimental data. M.P. conceived the simulations. F.B. and G.S. performed and analyzed the simulations. C.D. developed the FAST movie analysis software. L.L.P., C.A., M.M., M.P., and G.C. discussed the results. L.L.P., C.A., M.P., G.C. co-wrote the paper. All authors revised the manuscript. **Competing interests:** None declared. **Data and materials availability:** All data are reported in the main text and supplementary materials.

SUPPLEMENTARY MATERIALS

www.sciencemag.org/content/359/6381/1243/suppl/DC1
Materials and Methods
Figs. S1 to S8
Movies S1 and S2
References (*28*–*31*)

1 June 2017; resubmitted 4 December 2017
Accepted 25 January 2018
10.1126/science.aan8782

Real-time imaging of adatom-promoted graphene growth on nickel

Laerte L. Patera, Federico Bianchini, Cristina Africh, Carlo Dri, German Soldano, Marcelo M. Mariscal, Maria Peressi and Giovanni Comelli

Science **359** (6381), 1243-1246.
DOI: 10.1126/science.aan8782

Watching graphene grow

The growth of graphene on metal surfaces can be catalyzed by mobile surface metal atoms. Patera *et al.* used a high-speed scanning tunneling microscope to image the growth of graphene islands on a nickel surface. High temperatures caused carbon to diffuse to the surface, where mobile nickel atoms catalyzed graphene growth on the edges of islands. Molecular dynamics and density functional theory calculations provide mechanistic insights into the reaction steps.

Science, this issue p. 1243